ACS APPLIED MATERIALS & INTERFACES

Research Article

www.acsami.org

Tuning the Activity of Oxygen in $LiNi_{0.8}Co_{0.15}Al_{0.05}O_2$ Battery Electrodes

Khim Karki,[†,‡] Yiqing Huang,[†] Sooyeon Hwang,[‡] Andrew D. Gamalski,[‡] M. Stanley Whittingham,[†] Guangwen Zhou,[*,†] and Eric A. Stach[*,‡]

[†]NECCES, Binghamton University, Binghamton, New York 13902, United States

[‡]Center for Functional Nanomaterials, Brookhaven National Laboratory, Upton, New York 11973, United States

Supporting Information

ABSTRACT: Layered transition metal oxides such as $LiNi_{0.8}Co_{0.15}Al_{0.05}O_2$ (NCA) are highly desirable battery electrodes. However, these materials suffer from thermal runaway caused by deleterious oxygen loss and surface phase transitions when in highly overcharged and overheated conditions, prompting serious safety concerns. Using in situ environmental transmission electron microscopy techniques, we demonstrate that surface oxygen loss and structural changes in the highly overcharged NCA particles are suppressed by exposing them to an oxygen-rich environment. The onset temperature for the loss of oxygen from the electrode particle is delayed to 350 °C at oxygen gas overpressure of 400 mTorr. Similar heating of the particles in a reducing hydrogen gas demonstrated a quick onset of oxygen loss at 150 °C and rapid surface degradation of the particles. The results reported here illustrate the fundamental mechanism governing the failure processes of electrode particles and highlight possible strategies to circumvent such issues.

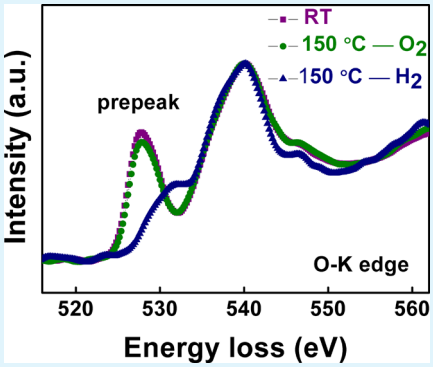

KEYWORDS: *chemical potential, oxidation−reduction, transition metal oxides, lithium-ion battery, transmission electron microscopy*

INTRODUCTION

Lithium-ion batteries (LIBs) have been predominantly used in consumer electronics and other power devices. The drive to use LIBs in large-scale applications such as electric vehicles (EVs) and smart grid applications has spurred significant research activity, particularly concerning the cathode electrodes. The current cathode materials, $LiCoO_2$ (~140 mA h/g) or $LiFePO_4$ (~160 mA h/g), have lower energy densities and cannot match the capacities of the next generation of anode materials (e.g., Si, ~4200 mA h/g).[1,2] Transition metal (TM) oxides such as $LiNi_{0.8}Co_{0.15}Al_{0.05}O_2$ (NCA)—which is cheaper and has a discharge capacity ~ 200 mA h/g—have been actively pursued as potential replacements. However, NCA cathodes suffer from rapid capacity fade and thermal instability, thus raising serious safety concerns for use in LIB applications. For example, NCA in the over-delithiated state (typically >4.2 V) and/or in overheated conditions can lead to oxygen loss from the surface of the particles, which can abruptly react with solvents in the liquid electrolyte to cause catastrophic thermal runaway.[1−8] Furthermore, this oxygen loss is accompanied by reduction and rearrangement of transition metal (TM) ions (primarily Ni) in the structure leading to deleterious phase transitions: from the original layered ($R\bar{3}m$) → disordered spinel ($Fd\bar{3}m$) → disordered rock salt ($Fm\bar{3}m$).[6,7] The disordered phases, particularly NiO-like rock-salt (RS) phase at the surface,[9] can lead to inhomogeneity of the transport of lithium ions and electrons into the bulk, resulting in lower capacity and poor rate capability of the electrode. Thus, it is critical to understand the mechanism that drives the loss of oxygen from the surface. Particularly, the environmental constraints that surround the particle (or electrode) surface can either catalyze or prevent severe oxygen activity at the surface of NCA, thus directly influencing the overall performance of the battery.

Previous studies have suggested that the overcharged or overheated condition can cause chemical and electrochemical decomposition of electrolyte solvents, creating a reducing environment at the electrode−electrolyte interface.[4,9−11] For example, $LiPF_6$ in ethylene carbonate and dimethyl carbonate can undergo an oxidative reaction to produce CO_2, H_2O, and H^+ ions. This results in electron exchange and extraction of Li^+ ions, which in turn leads to oxygen evolution from the surface. Likewise, the prolonged exposure of NCA particles to air (e.g., CO_2) or moisture (H_2O)—even in the absence of liquid electrolyte at room temperature—can form Li_2CO_3 or LiOH layers on the surface of the particles. This triggers oxygen loss.[12,13] Yang and co-workers[7,14] studied how temperature affects NCA electrodes at various states of charge (SOC) in a neutral helium gas environment through the use of time-resolved X-ray diffraction (TR-XRD), mass spectroscopy (MS), and X-ray absorption spectroscopy (XAS) techniques and found that the onset temperature for surface oxygen loss in overcharged conditions (~90% of lithium extracted) can occur

Received: August 4, 2016
Accepted: September 23, 2016
Published: September 26, 2016

DOI: 10.1021/acsami.6b09585
ACS Appl. Mater. Interfaces 2016, 8, 27762−27771

at 180 °C. Similar studies using spatially resolved transmission electron microscopy (TEM) in a high-vacuum environment showed that some oxygen loss and phase transition at individual overcharged particles can occur even at room temperature,[6,8,15] and can become severe at 150 °C.[15] Motivated by these observations, we systematically study the effect of various external stimuli on these processes. This includes the role of oxidizing, reducing and neutral environments on the surface oxygen loss, the role that the release of O_2 plays in the rearrangement of TM cations (Ni, Co) during the phase transformation, and the inherent mechanism to circumvent such losses. Specifically, we track the structural and electronic changes in the overcharged NCA particles at elevated temperatures in order to evaluate the onset temperature for oxygen loss and the overall thermal stability of the materials in oxidizing/reducing environments. In addition to creating the oxidizing/reducing environments at the elevated temperature (i.e., the thermodynamic driving force for phase transitions), the purpose of using high temperatures is to enhance the reaction kinetics. Elevated temperature can have a similar effect on an electric field during charging and discharging of a battery. This is because of the following: (1) the high temperature enhances ion migration and thus the kinetics of oxygen loss,[16] and (2) the migration of ions in LIBs during cycling is accelerated under the action of an electrical field in addition to a concentration gradient.[17] While the driving forces are different (thermal versus electric field), their effect is similar (i.e., enhancing the reaction kinetics).

In this report, we use in situ environmental TEM (ETEM) to study the effect of oxidizing (O_2), neutral (He), and reducing (H_2) gases on the oxygen loss and TM cation rearrangements that occur at the surface region of electrochemically charged NCA particles at elevated temperatures. ETEM provides a unique platform for these studies, as individual nanomaterials can be investigated for morphological, structural, or chemical changes, under external stimuli, in real time. Furthermore, an aberration-corrected ETEM with a differential pumping apparatus[18] allows a high spatial resolution of <0.1 nm, even in the presence of a high-pressure gas environment (e.g., O_2 and H_2). We have used in situ electron energy loss spectroscopy (EELS) of the overcharged NCA particles to investigate the surface chemistry of the samples in various environments, and we find that at an oxygen overpressure of 400 mTorr, the onset temperature for the surface oxygen loss is significantly delayed (350 °C). Conversely, upon introduction of reducing hydrogen gas, we observed quick loss of oxygen as early as 150 °C. The changes in the EELS spectra are also accompanied by surface structural changes, which we track through the use of the in situ high-resolution TEM (HRTEM) imaging. The results presented here provide fundamental insights into the surface characteristics of NCA cathode particles when subjected to varying environmental constraints such as oxidizing and reducing gas atmospheres and different temperatures. Furthermore, the robust demonstration that NCA particles can retain structural integrity in the presence of oxygen enrichment—even at extreme conditions (e.g., overcharged and overheating)—suggests that synthetic methods which suppress oxygen loss will lead to improvements in the performance and safety of NCA-based battery electrodes.

EXPERIMENTAL SECTION

Electrochemical Testing. $Li_xNi_{0.8}Co_{0.15}Al_{0.05}O_2$, also referred to as NCA, was commercially obtained from TODA America, Inc. The composite electrodes were prepared using a mixed slurry of 80 wt % active material, 10 wt % conducting carbon, and 10 wt % poly(vinylidene difluoride) (PVDF) binder in *N*-methylpyrrolidone (NMP) solvent. The mixed slurry was then cast onto an Al foil that acted as a current collector. The 2325-type of coin cell was prepared inside the Ar-filled glovebox with typical active material loading of 5 mg/cm^2, Li metal as the negative electrode, a Celgard separator, and an electrolyte of 1 M $LiPF_6$ dissolved in 1:1 ethylene carbonate (EC)/dimethyl carbonate (DMC) volume ratio. The electrochemical cell testing was performed using a battery cycler, MPG2 multichannel potentiostat (Biologic). The cells were delithiated to an overcharged state (x = 0.1) at a rate of $C/10$ using a galvanostatic condition (constant current). The amount of remaining lithium was estimated by the charge capacity, where 250 mA h/g corresponds to 90% state of charge. The galvanostatic charge profile is shown in the Supporting Information (Figure S1). The sample was charged to 4.7 V, and no discharging was performed.

Sample Preparation. The electrochemically overcharged electrode was immersed in DMC solution to remove the residual salts. The powder particles were collected by gently scraping the Al foil with a clean knife inside the glovebox. The powder electrodes were dissolved in the isopropyl alcohol (IPA) and sonicated for a few minutes to thoroughly disperse the particles. The solution of particles was simultaneously drop-cast onto either the conventional TEM lacey carbon grid or onto a MEMS-based EMheaterchip (DENS Solutions).[19] The heating experiments were performed using DENSsolutions' single-tilt holder. The EMheaterchip consists of a EMmicrohot plate which is 20 μm wide and 150 nm thick with platinum heating spiral embedded in a 400 nm thick SiN sandwich. There are 20 nm SiN windows between the heating spirals and electron transparent areas for sample particle imaging and characterization. The heating chip is then mounted in a DENS Solutions' TEM holder. Both the sample preparation and the loading into the TEM holder were performed inside an argon-filled glovebox. The holder is quickly transferred to the TEM room in a hermetically sealed container and inserted into prepumped goniometer with minimal air exposure (~2−3 s).

Environmental Transmission Electron Microscopy. Ex situ characterization of NCA particles such as acquiring bright-field (BF) images and selected area electron diffraction (SAED) patterns at room temperature were performed with a JEM 2100F instrument (JEOL), operating at an acceleration voltage of 200 kV. In situ heating of overcharged NCA particles were performed with an aberration-corrected Titan 80-300 (FEI) operated at 300 kV and equipped with a differential pumping system[18] that allows a gaseous atmosphere in the sample column. The gases−oxygen (oxidizing), helium (neutral), and hydrogen (reducing) were introduced into the sample particles at two desired partial pressures: 0.2 and 400 mTorr. The temperature in the sample region of the holder was controlled by DENSsolutions' Digiheater software interface connected to the Heater Control Box. The box communicated with the EMheaterchip via the contact between the four electrical pads of the chip and the four electrical contact pins of the holder. The temperature was determined by measuring the electrical resistance of the thin platinum spiral with a four-point probe method, and the readings were displayed on the software interface. The small dimensions of the heating element provide localized heating of the particles with a settling time of less than a second and a minimum mechanical drift (less than 1 nm/min at 800 °C). The sample particles were heated to the desired temperature and held for 2−3 min to reach thermal equilibrium before imaging. The beam was blanked at all times, except during the imaging process, to minimize beam-related damages on the particles.

Electron Energy Loss Spectroscopy. TEM-EELS was performed to obtain O-K, Co-$L_{2,3}$, and Ni-$L_{2,3}$ edges using a GIF Tridiem spectrometer (Gatan Inc.) The spectra were obtained from the same regions of interest from multiple particles. All spectra were referenced with the position of the zero loss peak (ZLP). The energy resolution as determined by measuring the full width at half-maximum of the ZLP was about 1 eV. The background subtraction for all spectra were performed with a freely available Athena (Demeter) package, which

DOI: 10.1021/acsami.6b09585
ACS Appl. Mater. Interfaces 2016, 8, 27762−27771

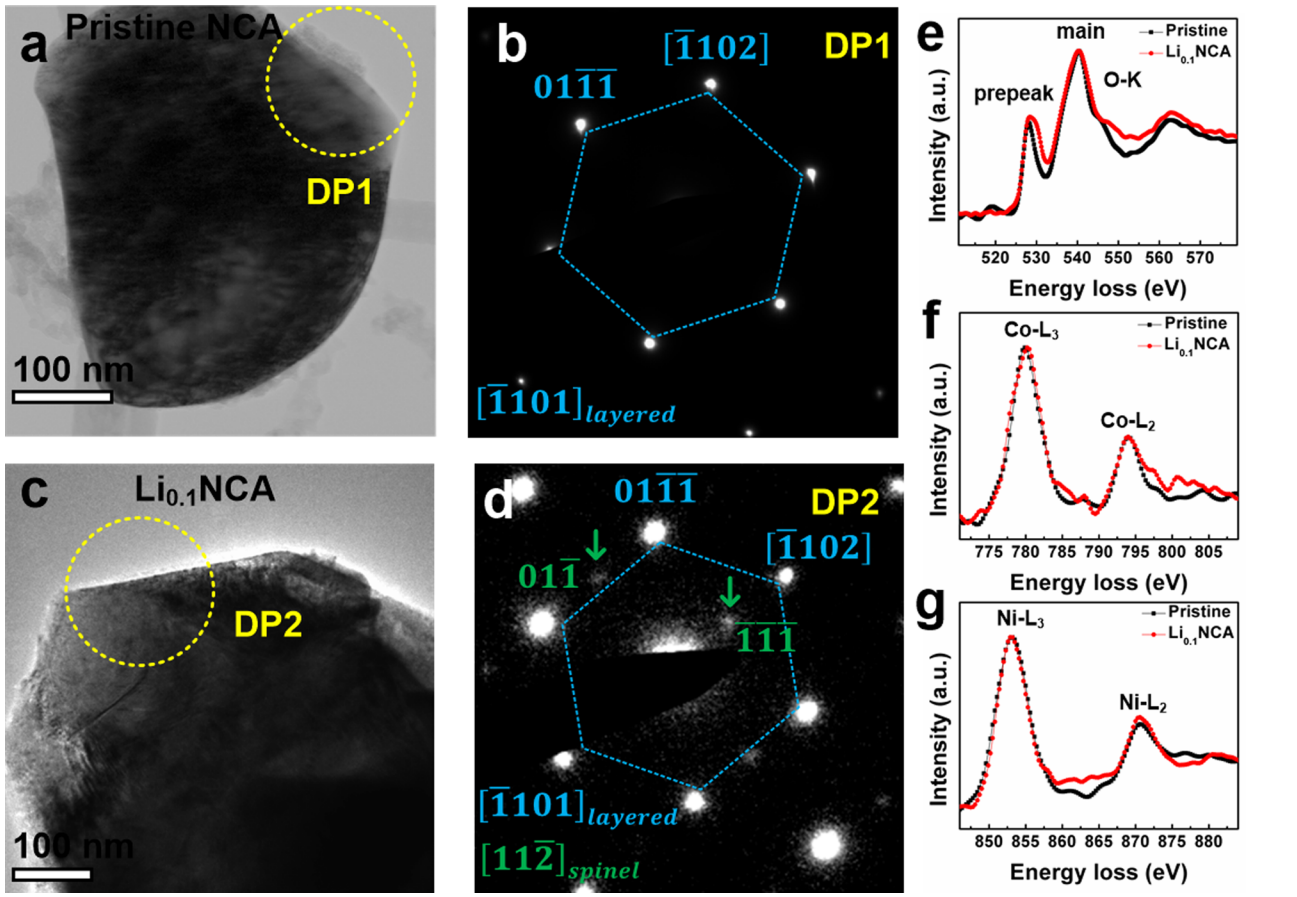

Figure 1. Characterization of pristine and overcharged NCA particles. (a) BF image of pristine NCA with corresponding electron diffraction (b) taken from surface DP1 area of panel a. The electron diffraction pattern clearly shows the layered ($R\bar{3}m$) structure at this stage. (c) TEM image of overcharged NCA particle with corresponding electron diffraction pattern (d) taken from surface DP2 area of panel c. The SAED spots suggest the presence of both the layered ($R\bar{3}m$) and spinel ($Fd\bar{3}m$) structures. TEM-EELS spectra of the pristine and overcharged NCA showing (e) O-K, (f) Co-$L_{2,3}$, and (g) Ni-$L_{2,3}$ edges.

used pre-edge line fitting, postedge curve fitting, and edge-step normalization techniques. The Ni-L_3/L_2 ratio were estimated using the white-line maximum intensity method; the details of which are given in refs 24 and 25. Any shifts in the position and the intensity of L_3 and L_2 peaks determine the d-band occupancy and the valence state of the transition metal ions.

RESULTS AND DISCUSSION

Pristine versus Overcharged NCA. Pristine NCA crystallizes in the layered ($R\bar{3}m$) structure, in which lithium and TM cations occupy the alternating octahedral layer sites (3a and 3b, respectively) between the cubic close-packed oxygen layers (6c) in an ABCABC stacking sequence. It is the migration of cations (Li^+ and TM ions) to either the tetrahedral or octahedral sites of the same oxygen framework that leads to the phase transformation from layered ($R\bar{3}m$) → disordered spinel ($Fd\bar{3}m$) → disordered RS ($Fm\bar{3}m$). During the phase transformation from the layered phase to the spinel, Li^+ cations occupy the 8a tetrahedral sites while the TM cations occupy the 16d octahedral sites. Upon further transition to the RS phase, both Li^+ cations and TM cations randomly occupy the octahedral sites. Figure 1a presents a low-magnification TEM-BF image of a typical pristine NCA particle. The particles are mostly irregular in shape, and the size varies from ~200 nm to 1.5 μm in length, with sufficiently thin electron transparent edges (~50 nm) on the surface. We concentrate on the surface region of the particles as the oxygen loss and the phase transformations initiate predominantly from the surface and propagate from the near-surface to the bulk of the particles,[6,8,15,20] supposedly in a core−shell pattern.[6] The SAED pattern in Figure 1b, extracted from the marked area (DP1) of the pristine particle (Figure 1a), shows sharp reflections indicating the well-ordered layered $R\bar{3}m$ structure viewed along the [$\bar{1}$101] zone axis. However, if 90% of the lithium (Li_xNCA, $x = 0.1$) is extracted from the particles, which we refer to as the "overcharged" state, we observe structural inhomogeneity and phase transformation on the surface of the most of the particles, consistent with prior reports.[8] Figure 1c is a typical TEM image of the overcharged NCA ($Li_{0.1}NCA$) at room temperature. The corresponding SAED pattern obtained from the marked area (DP2) in Figure 1c is shown in Figure 1d. The SAED pattern has dominant spots from the layered structure, with hexagonal symmetry when viewed along the [$\bar{1}$101] zone axis. Additionally, there are faint spots indicated by green arrows, which can be indexed to the spinel structure along the [11$\bar{2}$] zone axis. The observation of additional spots indicates that there is a mixed structure, having both the layered and spinel structures on the surface. Such spinel-like transformation on the surface region of the overcharged NCA is commonly observed, even at room temperature.[6,8,15] First principle calculations attribute this room-temperature phase transformation to kinetics driven by cation mobility and vacancies generated during delithiation, although a thermody-

DOI: 10.1021/acsami.6b09585
ACS Appl. Mater. Interfaces 2016, 8, 27762−27771

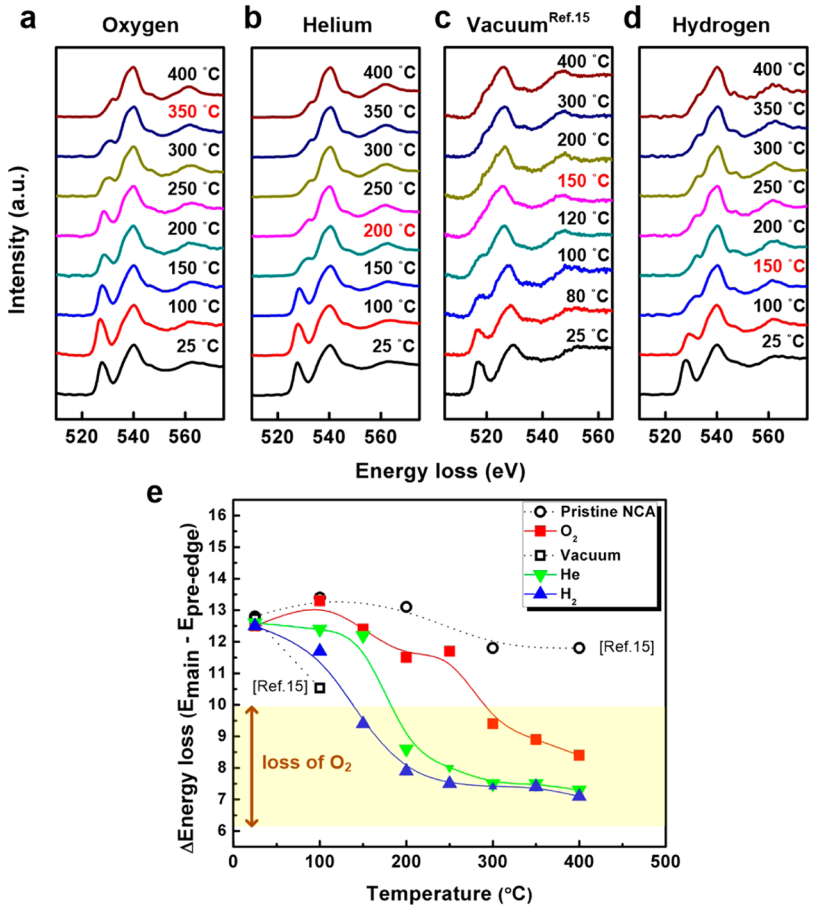

Figure 2. Temperature-dependent oxygen evolution of the overcharged NCA ($Li_{0.1}NCA$) particle observed at overpressurized oxidizing (O_2), neutral (He), and reducing (H_2) environments in the ETEM. (a) Evolution of O-K spectra as a function of temperature at P_{O_2} of 400 mTorr. Here, the O-K prepeak starts to fade (shift to the higher energy) at 350 °C. (b) When overcharged NCA is heated under the similar partial pressure (400 mTorr) of helium (neutral gas), the prepeak fades at 200 °C. (c) Overcharged NCA heated in a vacuum condition (data extracted from ref 15) shows the onset temperature of 150 °C. (d) In the reducing gas (H_2) environment, the prepeak of O-K edge fades quickly at 150 °C, indicating the reduction of (CoNi)O even at low temperatures. (e) Changes in energy loss ($\Delta E_{O\text{-}K}$) with increasing temperature in different gas environments. Note that the pristine NCA, extracted from ref 15, was heated in the vacuum environment of TEM.

namic driving force for this conversion is possible even at 0 K.[16,21] Upon cation relocation in the oxygen framework, the nearby coordination number and bonding with the oxygen are altered, triggering the change in the electronic state of NCA. To track these changes, we use EELS to probe the same areas where the SAED patterns are obtained, and compare absorption spectra from the O-K edge, Co-$L_{2,3}$ edges, and Ni-$L_{2,3}$ edges of both the pristine and overcharged NCA particles. Although XAS techniques provide higher energy resolution for studying the electronic state of such materials,[7,14,22,23] they provide average information, mostly from the bulk. Moreover, the phase transformation predominantly initiates from within the few nanometer range of the particle. EELS is therefore better suited for studying such localized changes. Figure 1e shows two distinct edges for the O-K spectra, which include a sharp pre-edge peak ("prepeak" from hereafter) at around 527−530 eV and a broad main-edge peak ("main-peak" from hereafter) at around 538−540 eV. The presence of a prepeak in the O-K spectra is a typical characteristic observed in the TM oxides.[24] The prepeak arises due to the transition of electrons from the O 1s state to unoccupied O 2p states, which then hybridize with the 3d state of the TM (primarily Ni), while the main-peak occurs due to the transition of electrons from the 1s state to hybridized O 2p and TM 4sp states.[8,22,24] The change in the intensity of O-K prepeak and/or difference in the energy ($\Delta E_{O\text{-}K}$) between the prepeak and main-peak can be directly correlated with the oxidation state of the TM ions.[22,24,25] Hence, the prepeak analysis provides information on the 3d occupancy or the oxidation state of the TM ions. All O-K edge spectra in Figure 1e and hereafter are aligned and normalized to the intensity of the main-peak. The slightly higher intensity of the prepeak in the case of overcharged NCA ($Li_{0.1}NCA$), compared to pristine NCA, is due to an increase in the oxidation state of TM ions (mostly Ni^{3+} oxidizes to Ni^{4+}) and charge compensation with the oxygen ions upon lithium extraction at the surface.[8,14,23] Likewise, L edges for Co and Ni typically show two characteristic peaks or white lines (L_3 and L_2) as shown in Figure 1f,g. The two peaks originate from the transitions of electrons from $2p_{3/2}$ and $2p_{1/2}$ core states to empty 3d states, which then hybridize with the 2p orbitals of oxygen in the oxide.[25−27] The difference in the energies of the two peaks is due to the spin−orbit coupling of the p-shell.[28] Interestingly, the white-line ratio between the L_3 and L_2 peaks has been shown to present a rough estimate of the valence (oxidation) state of the TM ions[25−27] (see Experimental Section). Figure 1f shows the Co-$L_{2,3}$ edges for both pristine and overcharged NCA. All Co-L_2 edge spectra in Figure 1f and hereafter are aligned and normalized to the intensity of the Co-

DOI: 10.1021/acsami.6b09585
ACS Appl. Mater. Interfaces 2016, 8, 27762−27771

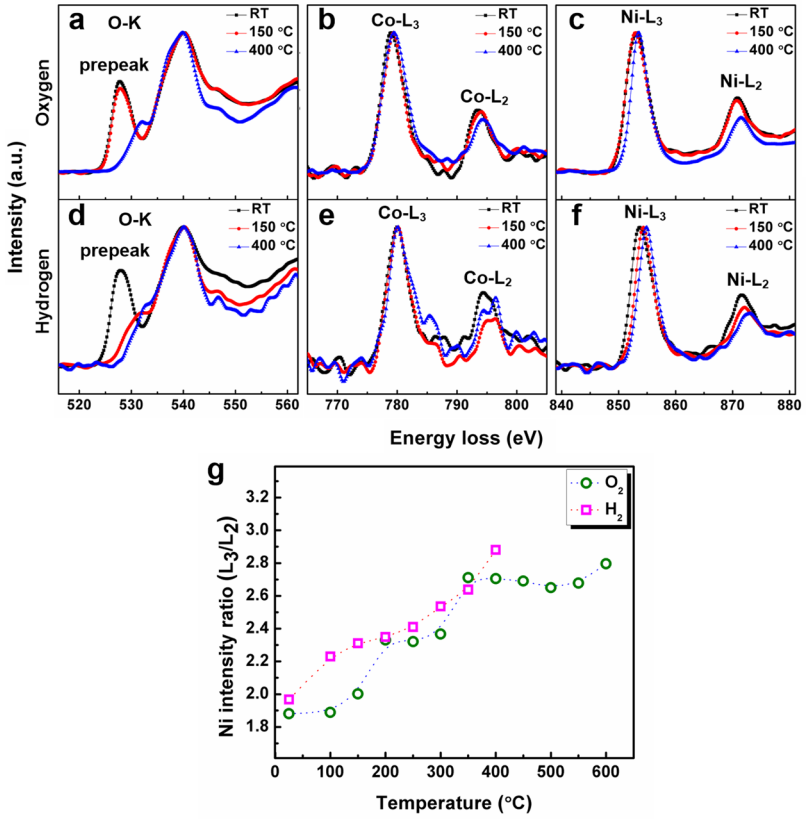

Figure 3. Correlating O-K spectra changes with corresponding Co-$L_{2,3}$ and Ni-$L_{2,3}$ edges in both oxidizing (O_2) and reducing (H_2) gas environments at RT, 150 °C, and 400 °C. (a–c) Spectral O-K, Co-$L_{2,3}$, and Ni-$L_{2,3}$ changes at P_{O_2} of 400 mTorr. (d–f) Similar EELS profiles showing changes in O-K, Co-$L_{2,3}$, and Ni-$L_{2,3}$ edges at P_{H_2} of 400 mTorr. (g) Summary of Ni (L_3/L_2) ratio measured as a function of temperature in O_2 and H_2 gas environments.

L_3 edges. The ratio of the Co-L_3 intensity to that of the Co-L_2 for both the pristine and the overcharged NCA shows no obvious changes, consistent with previous EELS analysis.[20] It should be noted that the stoichiometric composition for Co in the NCA is only 15%, which will prohibit enough EELS signals for accurate analyses from small areas. However, the bulk studies with high energy resolution XAS techniques have suggested that Co tends to be more stable upon its transition to the spinel phase, while Ni is relatively unstable and quickly reduces to form the RS phase.[7,29,30] Thus, this study focuses on tracking changes primarily in the Ni-L_2/L_3 edges. Figure 1g shows the Ni-$L_{2,3}$ edges for both pristine and overcharged NCA. All Ni-$L_{2,3}$ edge spectra in Figure 1g and hereafter are aligned and normalized to the intensity of the Ni-L_3 edges. The slightly lower Ni-L_3/L_2 ratio and higher tail intensity observed in both L_3 and L_2 edges of overcharged NCA over the pristine NCA is likely due to the oxidation of Ni^{3+} to Ni^{4+} state.[8,14,23] Several previous studies[6−9,15] have also demonstrated that the surface/subsurface regions of the overcharged NCA can act as the critical point of the electrode particles because of two major changes: (1) abrupt reduction occurs on the surface (primarily Ni^{4+}) even at room temperature, leading to release of oxygen and possible thermal runaway, and (2) the formation of the RS (NiO) phase causes severe rise in the impedance. Thus, we concentrate our effort in understanding the thermal behavior of NCA in the overcharged state at oxidizing (O_2), neutral (He) and reducing (H_2) gas environments. Most importantly, it is critical to understand the direct role that the overpressurized oxidizing and reducing gases can play in changing the overall oxygen chemical potential from the surface/subsurface regions of overcharged NCA particles at various temperatures.

ETEM Gas Overpressure Influencing the Oxidation and Reduction of Overcharged NCA. We track the evolution of O-K edges in the overcharged NCA particles (Figure 2a) as a function of temperature by flowing overpressurized oxygen gas at $P_{O_2} \approx 400$ mTorr. At room temperature (25 °C), the shape of the prepeak and main-peak resemble that of overcharged NCA, as shown in Figure 1e. Upon increase in temperature, the intensities of the prepeak gradually decrease, and the peak position shifts from lower to higher energies. The prepeak starts to fade significantly only when the temperature reaches around 350 °C and thereafter becomes a shoulder of the main-peak. The reduced intensity in the prepeak is a measure of stoichiometric oxygen loss (oxygen vacancy formation) from the surface of the particle, which occurs upon the reduction of TM ions and charge compensation with the oxygen ions.[16,24,28,30,31] This onset temperature for the prepeak fade is a conservative estimate and could potentially occur beyond that temperature. This is a significant improvement from a previously reported case in which the onset temperature for severe oxygen loss has been reported to occur quickly in the helium (≈180 °C)[7,14] or vacuum (150 °C)[15] environment. To corroborate with these reports, and to further verify that oxygen indeed played a role in suppressing the surface oxygen loss from the particle, we track O-K changes by flowing oxygen at a lower pressure of $P_{O_2} \approx 0.2$

DOI: 10.1021/acsami.6b09585
ACS Appl. Mater. Interfaces 2016, 8, 27762−27771

mTorr (Supporting Information, Figure S2) and at similar high helium gas overpressure (P_{He}) of ≈400 mTorr (Figure 2b). Interestingly, at $P_{O_2} \approx 0.2$ mTorr, the onset temperature for prepeak loss occurred early at 200 °C, confirming that, at less oxygen enrichment, the loss of oxygen is still significant. Helium is a neutral gas and should not facilitate any structural or chemical changes in the material. As shown in Figure 2b, the prepeak in the He environment fades at or beyond 200 °C, which approximately resembles the previous bulk-scale studies using helium.[7,14] However, this onset temperature is significantly lower than in the case of the higher oxygen overpressure (Figure 2a). In vacuum (≈10^{-7} Torr), the loss of the prepeak is shown to occur as early as 120 °C, and it completely vanishes at 150 °C (Figure 2c, the O-K profile is extracted from ref 15). Presumably the severity of oxygen loss in vacuum is because any oxygen from the surface is readily removed in the high-vacuum environment of the TEM. Upon verifying the improved stability of overcharged NCA in a highly oxidizing environment, we next perform a similar study in highly reducing environments. More practically, the oxidation of electrolyte solutions in both overcharged and overheated conditions is known to create a reducing environment at the electrode−electrolyte interface,[4,9−11] which further motivates these experiments. Figure 2d presents data from overcharged NCA that is heated in the presence of a reducing H_2 gas at the same partial pressure (P_{H_2}) of ≈400 mTorr. As anticipated, the loss of the O-K prepeak occurs at 150 °C, which is the worst among all the cases we study herein. In Figure 2e, we compare all of the above cases by plotting $\Delta E_{O\text{-}K}$ as a function of temperature. In the case of pristine NCA, which is replotted using data from ref 15, the changes in $\Delta E_{O\text{-}K}$ are not significant when it is heated to temperature around 400 °C in the vacuum environment. This suggests that there is no significant oxygen loss during this process. When the overcharged NCA is heated in the O_2 environment, the $\Delta E_{O\text{-}K}$ drops significantly only when it reaches a temperature at or beyond 300 °C. In the case of vacuum, $\Delta E_{O\text{-}K}$ drops relatively early, at or below 150 °C. The change in $\Delta E_{O\text{-}K}$ occurs earlier when the sample particle is heated in the reducing H_2 environment, suggesting an earlier loss of oxygen. Thus, it is evident that the fading of the prepeak correlates to the loss of oxygen from the surface of the particle, and it can be significantly suppressed at the higher oxygen enrichment.

To further demonstrate that the loss of oxygen has direct correlation with the reduction of TM ions (mostly Ni), we systematically compare the evolution of O-K edges with the corresponding Co-$L_{2,3}$ and Ni-$L_{2,3}$ edges performed at RT and 150 and 400 °C, in both the oxidizing and reducing gas environments. The observed changes in the intensity of the O-K prepeak and/or $\Delta E_{O\text{-}K}$ correlate with changes in the oxidation state of the TM ions.[8,14,23] For example, the evolution of $\Delta E_{O\text{-}K}$ in Figure 1e corresponds to changes in Co-$L_{2,3}$ and Ni-$L_{2,3}$ edges and identifies which among the transition metals in the mixed oxides undergoes significant reduction. Previous studies have shown that there is a linear correlation between $\Delta E_{O\text{-}K}$ and changes in TM oxidation states:[24,28,31] the observed decrease in the $\Delta E_{O\text{-}K}$ means that there is a reduction in the TM oxidation state. Panels a−c of Figure 3 present the evolution of the O-K, Co-$L_{2,3}$, and Ni-$L_{2,3}$ edges of overcharged NCA in oxidizing O_2 overpressure at RT and upon heating at 150 and 400 °C, respectively. The O-K prepeak of overcharged NCA after heating at 150 °C is still prominent, and there is only a slight reduction in the intensity compared to that of the RT peak. As expected, there are only slight changes in the Co-L_2 and Ni-L_2 intensities as well. At 400 °C, the intensity of the O-K prepeak decreases significantly, which would suggest the reduction of TM ions. The change in the intensity of Co-L_2 peak is minor, indicating that there is less reduction in Co, consistent with the previous study.[7] However, Ni-L_2 has reduced significantly. Additionally, the tails of the O-K main edge and the Ni-L_3 and the Ni-L_2 edges decrease significantly at 400 °C. When the overcharged NCA is heated in the presence of a reducing H_2 overpressure (Figures 3d−f), the loss in the O-K prepeak (Figure 3d) occurs quickly at 150 °C, which correlates with some reduction in the Co-L_2 edge (Figure 3e) and there is significant reduction in the Ni-L_2 (Figure 3f) edge. At 400 °C, the O-K prepeak reduces significantly and becomes a shoulder of the main-peak. The intensities of both Co-L_2 and Ni-L_2 reduce as well. The changes in the Ni L_3/L_2 ratio for overcharged NCA upon heat treatment in the oxidizing and reducing environments as a function of temperature are shown in Figure 3g. The Ni L_3/L_2 ratio for overcharged samples at room temperature (Figure 1g) is expected to be around 1.8−2.0.[15] As the temperature increases, the reduction of the TM ions causes the Ni-L_3/L_2 ratio to increase to around 2.5−3.5.[15,32] Figure 3g shows that such an increase in the L_3/L_2 ratio occurs rapidly at around 100 °C in the reducing environment and increases linearly upon further heat treatment. However, there is a slow increase in the L_3/L_2 ratio for the oxidizing environment, up to 200 °C, which then increases further in a plateau-like manner. Clearly, there is a direct correlation between the fading of the O-K prepeak and the reduction of the TM cations—predominantly Ni—on the surface region of the overcharged NCA. Furthermore, there is a delay in the loss of the O-K prepeak in the oxidizing environment, which is also concomitant with the delay in the increase in the Ni-L_3/L_2 ratio. The abrupt reduction of the O-K prepeak and early increase in the Ni-L_3/L_2 ratio—even at the low temperature in the reducing H_2 environment—is due to a higher rate of Ni^{4+} reduction to $Ni^{3+/2+}$.

The delay in the release of lattice oxygen from the bulk is governed by both thermodynamic and kinetic factors, primarily the changes in the oxygen chemical potential between the gas and the solid surface of the particle.[16,33] The adsorption and desorption of gas species on the immediate surface of the particle determines the chemical potential difference ($\Delta\mu^O$) between oxygen in the gas equilibrium phase (μ_g^O) and the bulk NCA equilibrium phase (μ_s^O), such that $\Delta\mu^O = (\mu_s^O - \mu_g^O) = -\frac{1}{2}kT \ln\left(\frac{P_{O_2}}{P^e_{O_2}}\right)$,[33,34] where k is the Boltzmann constant, T, P_{O_2}, and $P^e_{O_2}$ represent temperature, actual oxygen pressure in the gas phase, and the equilibrium oxygen pressure for NCA, respectively. At lower temperatures, NCA likely maintains a stoichiometric composition and remains in its most stable state. Upon heating in the presence of flowing oxygen at the higher P_{O_2} of 400 mTorr (Figure 2a), the surface adsorption of oxygen from the gas phase appears to compensate for the oxygen loss from the NCA. Ideally, as P_{O_2} increases, $\Delta\mu^O$ approaches zero and the surface loss of oxygen from the NCA becomes less favorable thermodynamically. At the overpressure of 400 mTorr, the onset temperature for the fading in intensity of the O-K prepeak (oxygen loss) is significantly delayed to 350 °C. With a lower P_{O_2} of 0.2 mTorr

DOI: 10.1021/acsami.6b09585
ACS Appl. Mater. Interfaces 2016, 8, 27762−27771

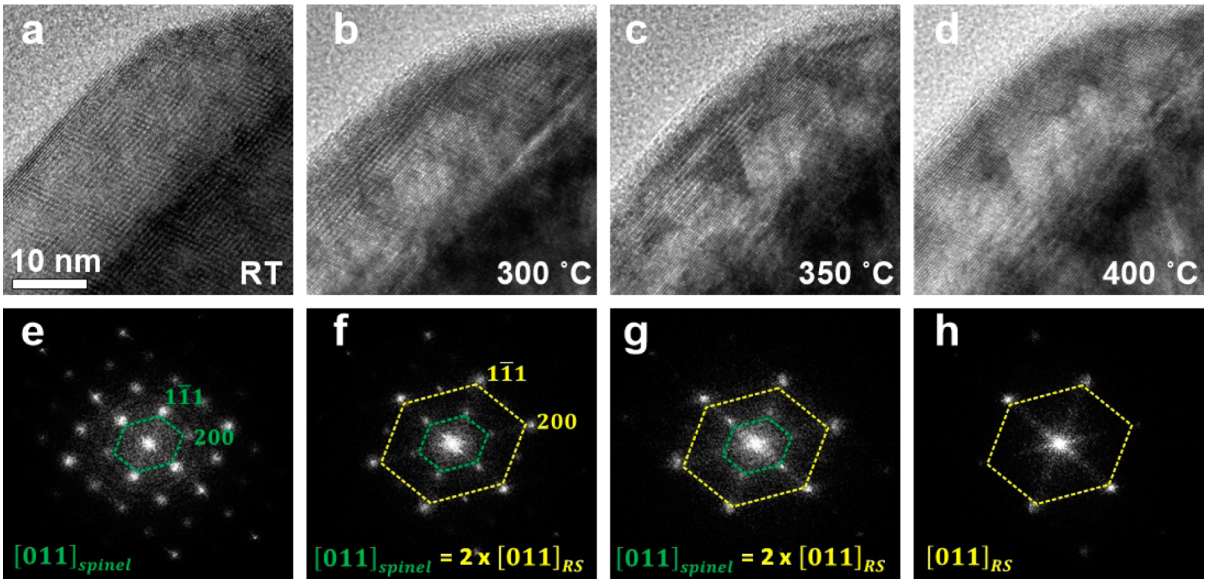

Figure 4. Tracking structural phase transformation with increasing temperature at P_{O_2} of 400 mTorr. (a) HRTEM image of an overcharged NCA particle at room temperature (RT) with corresponding diffractogram shown in panel e. As shown by the diffraction spots in panel e, the surface structure of NCA at RT is predominantly spinel-like (green hexagon). (b) At 300 °C, there is slight roughening in the morphology at the surface. The corresponding diffractogram (f) shows prominent spots designated to the RS-like structure (yellow hexagon), while the spots for the spinel-like structure appear faint. As shown in EELS profile in Figure 2a, the O-K prepeak starts to disappear at this temperature, suggesting that the oxygen loss can be related to the spinel → RS phase transformation. (c) At 350 °C, the surface of the NCA particle undergoes more roughening. The corresponding diffractogram (g) shows weakened spinel spots, while the spots for the RS phase become dominant. This occurs at the same point when the shoulder of the O-K prepeak (Figure 2a) becomes rather plateaued. (d) At 400 °C, the surface is completely transformed to the RS phase (h), and there are no spots featuring any spinel-like structure, although the RS spots become dominant.

(Supporting Information, Figure S2), the O-K pre-edge fades early at 200 °C, although this is a modest improvement over the neutral He gas at higher partial pressure ($P_{He} \approx 400$ mTorr). In the case of He gas ($P_{He} \approx 400$ mTorr), the adsorption of neutral gas species cannot compensate for any loss of surface oxygen from bulk NCA upon heating and the O-K prepeak disappears at 200 °C, which is comparable to the case in lower P_{O_2}. In the case of vacuum, although the thermodynamic driving force for oxygen loss should theoretically remain the same as in the He case, any loss of oxygen from the NCA surface will be quickly evacuated from the surface by the vacuum environment of TEM, and the O-K prepeak fades slightly early at 150 °C. In the reducing H_2 environment, oxygen from the surface is swiftly consumed[35] (presumably to form moisture), prompting drastic reduction of the TM ion to its metallic form (particularly Ni).[36] The rapid increase of the Ni (L_3/L_2) ratio in P_{H_2} compared to P_{O_2} (Figure 3g) suggests that the Ni^{4+} in the NCA undergoes reduction to Ni^{2+} (or even Ni^0) rather quickly in the low-temperature regime.

Structural Phase Transformations with Temperature. To corroborate the observed changes in electronic structure with structural transformations in the oxidizing and reducing gases, we also perform in situ HRTEM analyses of the surface region of overcharged NCA. Figure 4 shows the surface structural evolution of overcharged NCA upon heating in the oxygen overpressure. At RT, the surface of the particle has already transformed to the spinel phase, as is generally expected in such a highly overcharged state.[6,8,15] The diffractogram of the viewed area (i.e., a fast Fourier transform or FFT of the HRTEM image in the region indicated in Figure 4a), which is shown in Figure 4e, has strong reflections (green hexagon) that corresponds to the [011] spinel zone axis. When the temperature reaches 300 °C (Figure 4b)—which is the point when the O-K prepeak diminishes (Figures 2 and 3)—some surface roughening is observed. From the corresponding diffractogram in Figure 4f, it is evident that the reflections corresponding to the RS phase (yellow hexagon) oriented in the [011] zone axis become dominant over the spinel reflections. It should be noted that the lattice parameter of spinel is twice as large as that of the RS structure. Thus, the evolution of spot intensity represented by yellow hexagon is an indicator of phase transformation from spinel to RS phase. Indeed, the dominance of RS reflections suggests that the surface edge of the particle has undergone a nearly complete phase transformation, accompanied by the loss of oxygen. At 350 °C (Figure 4c), the reflections for the spinel phase (Figure 4g) further diminish and the RS phase becomes dominant. At 400 °C (Figure 4d), no spinel reflections are visible from the diffractogram in Figure 4h. The surface morphology of the particle further degrades as well.

In contrast to the oxidizing environment, the heating of overcharged NCA particles in the reducing H_2 environment dramatically changes both the electronic state (Figure 2 and Figure 3) and the nature of the structural phase transformation. Figure 5a shows a low-magnification TEM image of the NCA particle at RT. If we zoom in to the surface of the particle, as marked by the blue frame, the immediate surface area of the particle (~2–3 nm) shows a different lattice structure from the bulk (Figure 5b), and the corresponding diffractogram taken from the area in the yellow frame shows reflections corresponding to the RS phase along the [011] zone axis. The near-surface region is predominantly spinel, as is evident from the reflections extracted from the green framed area, and is indexed to the [11$\bar{2}$] zone axis. However, when the particle is

DOI: 10.1021/acsami.6b09585
ACS Appl. Mater. Interfaces 2016, 8, 27762–27771

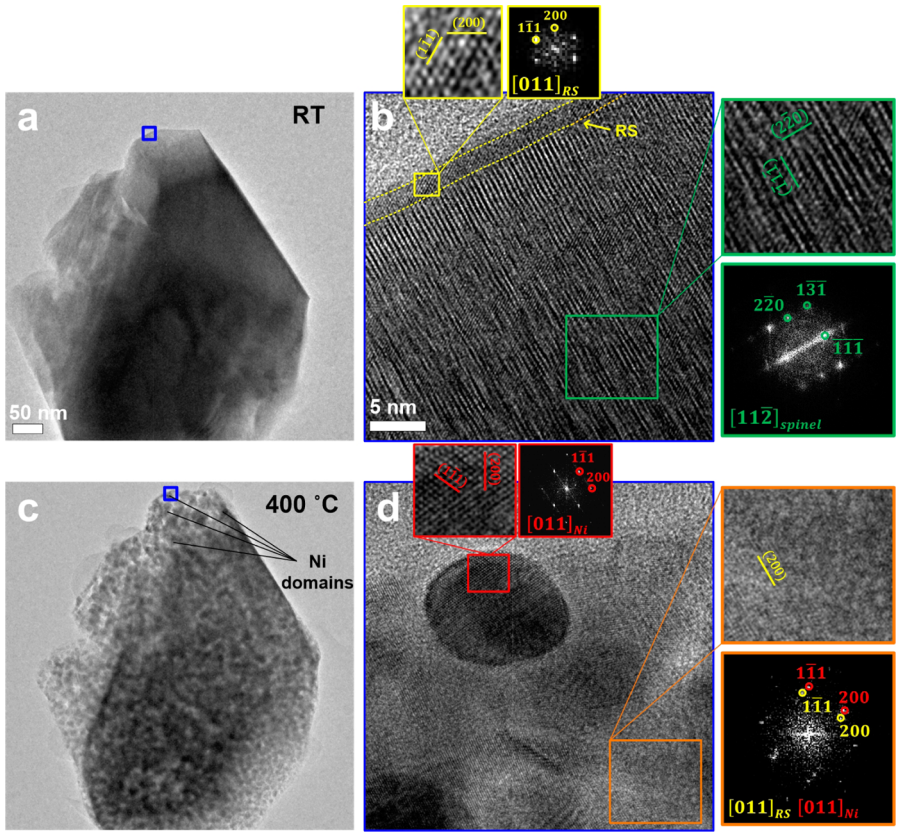

Figure 5. HRTEM analysis of overcharged NCA particle in the H_2 environment (P_{H_2} of 400 mTorr) at RT and 400 °C. (a) Morphology of NCA at room temperature. (b) Magnified image taken from the surface of the particle (blue box) in panel a. Again, the surface shows RS-like features (FFT from yellow boxed area). The near-surface region is spinel-like, as shown by the magnified region of the HRTEM image and the FFT from the green boxed area. (c) Compared to the O_2 environment, the particle in the H_2 environment degrades rapidly, as early as 400 °C. The low-magnification image shows granular-like domains on the surface of the particle, which suggests the further reduction of NiO to form Ni nanodomains. (d) Further magnification of the blue boxed area shown in panel c. There are Ni domains scattered on the surface. From the FFT (red box), the structure shows features of metallic Ni. Upon inspection by FFT in the orange box area, the structure shows features both from NiO and metallic Ni structure, though with some degree of rotation (~3–6°).

examined at 400 °C (Figure 5c), the surface appears granular, as is typically observed during the reduction of metal oxide.[32,37] Upon closer examination (Figure 5d; Supporting Information Figure S3), the grains appear to be metallic Ni. An FFT of the lattice fringes from the red frame area of the particle shows reflections corresponding to Ni in the [011] zone axis. A similar FFT pattern from the yellow framed area shows a difference in the lattice fringe spacing, which can be indexed to Ni and NiO (RS phase) and are aligned with a rotation of ~3–6°. The coherency of the FFT spots between the Ni and NiO (albeit with some rotational difference) suggests that the Ni nucleates over NiO by forming a loosely epitaxial relationship.[32] The angular difference between the Ni and NiO reflections results from the presence of dislocations in the Ni domains.[38] Such isolation of inactive Ni domains on the surface is likely responsible for the rise in the interfacial impedance and the significant capacity loss from the electrode.[9]

Compared to the deleterious effect of overcharged NCA under the H_2 partial pressure, similar heating in the O_2 environment at the temperature as high as 600 °C shows no apparent coarsening of the particles. Figure 6a presents a low-magnification image of the NCA at RT. Upon heating to 600 °C (Figure 6b), there is some roughening on the surface but no granular-like features are present. Close examination of the blue frame area of the particle taken from Figure 6a at RT shows about 2–3 nm of RS phase at the immediate surface area (Figure 6c), which is commonly observed in overcharged NCA.[8,15] The FFT pattern in the yellow frame area (box 1) shows reflections for the [011] zone axis of the RS phase. The near-surface region shows pristine lattice fringes for the spinel phase. The FFT pattern from the green frame area (box 2) shows reflections for spinel along the [011] zone axis. At 400 °C (Figure 6d), both the surface and the near-surface area undergo phase transformation. The FFTs from boxed areas "3" and "4" show reflections from the RS phase. At 600 °C (Figure 6e), the morphology of the particle surface changes significantly. However, the FFTs from the boxed areas "5" and "6" show prominent lattice fringes from the RS phase. In stark contrast to the reducing H_2 gas environment, Ni segregation is not observed, even at such extreme temperatures. From these observations, it is clear that oxygen enrichment prevents the NCA particle from the rapid degradation by delaying the permanent loss of oxygen from the structure and leads to reconstruction of the surface.

CONCLUSIONS

In conclusion, we have demonstrated that environmental constraints, such as oxidizing or reducing environment can have a direct impact on the surface oxygen loss and the concomitant phase transformations that occur in NCA-based

DOI: 10.1021/acsami.6b09585
ACS Appl. Mater. Interfaces 2016, 8, 27762–27771

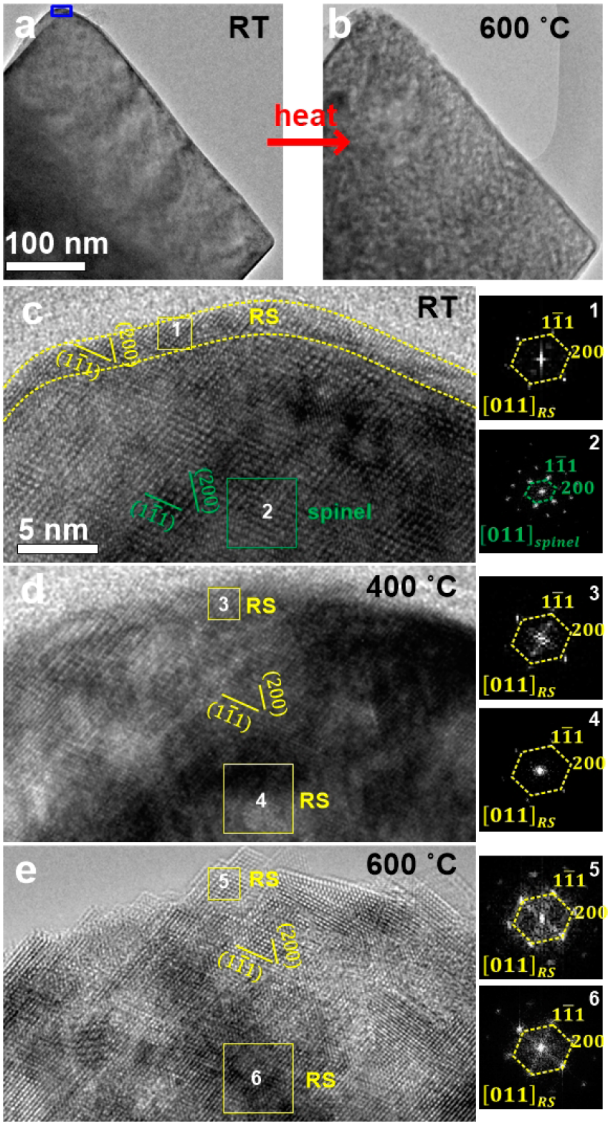

Figure 6. HRTEM analysis of overcharged NCA particle in the O_2 environment (P_{O_2} of 400 mTorr) at RT and 600 °C. Morphology of the overcharged NCA at (a) room temperature and (b) 600 °C. (c) High-magnification image taken from the surface edge (marked in blue box) in panel a. Based on the FFT taken from boxed "1" and "2" areas of panel c, the top surface edge of the NCA has RS structure, while the near-surface region is predominantly spinel. (d) At 400 °C, the surface and near-surface regions of the particle appear roughened. The FFTs from both boxed areas "3" and "4" show reflections for the RS phase. (e) Upon heating the sample to 600 °C in the higher O_2 pressure (≈400 mTorr), both the surface and the near-surface regions completely transform into the RS phase (see FFT "5" and "6").

cathode materials. Furthermore, the robust behavior of NCA particles at higher P_{O_2}, even at extreme heating conditions (600 °C), suggests that the creation of a compatible surface environment (such as robust battery electrolyte[39] or appropriate surface modifications[40,41] of the electrodes) to suppress oxygen loss could be a viable option for successful utilization of NCA-based battery electrodes. Such a strategy could be extended to other TM oxide based battery cathode materials such as $LiNi_xMn_{1-x-y}Co_yO_2$ (NCM), which more or less suffer from similar surface degradation effects.[6,14,30,42,43] Furthermore, the real-time insights of surface oxidation and reduction processes observed in our study may be applied to understand the atomic scale effects of a reducing and oxidizing chemical potential on the surface of other energy-related materials, such as lithium−air batteries, catalysts, and solid oxide fuel cells.

■ ASSOCIATED CONTENT

Supporting Information

The Supporting Information is available free of charge on the ACS Publications website at DOI: 10.1021/acsami.6b09585.

Galvanostatic charge (delithiation) of the NCA particles, oxygen evolution of overcharged NCA at lower P_{O_2} of 0.2 mTorr as a function of temperature, and another case of overcharged NCA particles heated in the H_2 environment at P_{H_2} of 400 mTorr (PDF)

■ AUTHOR INFORMATION

Corresponding Authors

*E-mail: gzhou@binghamton.edu (G.Z.).
*E-mail: estach@bnl.gov (E.A.S.).

Notes

The authors declare no competing financial interest.

■ ACKNOWLEDGMENTS

This work is supported as part of the NorthEast Center for Chemical Energy Storage (NECCES), an Energy Frontier Research Center funded by the U.S. Department of Energy (DOE), Office of Science, Basic Energy Sciences under Award No. DE-SC0012583. This research used resources of the Center for Functional Nanomaterials, which is a U.S. DOE Office of Science Facility, at Brookhaven National Laboratory under Contract No. DE-SC0012704, which also funded E.A.S.

■ REFERENCES

(1) Whittingham, M. S. Lithium Batteries and Cathode Materials. *Chem. Rev.* **2004**, *104* (10), 4271−4302.

(2) Doeff, M. Battery Cathodes. In *Batteries for Sustainability SE-2*; Brodd, R. J., Ed.; Springer: New York, 2013; pp 5−49, DOI: 10.1007/978-1-4614-5791-6_2.

(3) Belharouak, I.; Lu, W.; Vissers, D.; Amine, K. Safety Characteristics of $Li(Ni_{0.8}Co_{0.15}Al_{0.05})O_2$ and $Li(Ni_{1/3}Co_{1/3}Mn_{1/3})O_2$. *Electrochem. Commun.* **2006**, *8* (2), 329−335.

(4) Armstrong, A. R.; Holzapfel, M.; Novák, P.; Johnson, C. S.; Kang, S.-H.; Thackeray, M. M.; Bruce, P. G. Demonstrating Oxygen Loss and Associated Structural Reorganization in the Lithium Battery Cathode $Li[Ni_{0.2}Li_{0.2}Mn_{0.6}]O_2$. *J. Am. Chem. Soc.* **2006**, *128* (26), 8694−8698.

(5) Kim, Y.; Cho, J. Lithium-Reactive $Co_3(PO_4)_2$ Nanoparticle Coating on High-Capacity $LiNi_{0.8}Co_{0.16}Al_{0.04}O_2$ Cathode Material for Lithium Rechargeable Batteries. *J. Electrochem. Soc.* **2007**, *154* (6), A495−A499.

(6) Wu, L.; Nam, K.-W.; Wang, X.; Zhou, Y.; Zheng, J.-C.; Yang, X.-Q.; Zhu, Y. Structural Origin of Overcharge-Induced Thermal Instability of Ni-Containing Layered-Cathodes for High-Energy-Density Lithium Batteries. *Chem. Mater.* **2011**, *23* (17), 3953−3960.

(7) Bak, S.-M.; Nam, K.-W.; Chang, W.; Yu, X.; Hu, E.; Hwang, S.; Stach, E. A.; Kim, K.-B.; Chung, K. Y.; Yang, X.-Q. Correlating Structural Changes and Gas Evolution during the Thermal Decomposition of Charged $Li_xNi_{0.8}Co_{0.15}Al_{0.05}O_2$ Cathode Materials. *Chem. Mater.* **2013**, *25* (3), 337−351.

(8) Hwang, S.; Chang, W.; Kim, S. M.; Su, D.; Kim, D. H.; Lee, J. Y.; Chung, K. Y.; Stach, E. A. Investigation of Changes in the Surface Structure of $Li_xNi_{0.8}Co_{0.15}Al_{0.05}O_2$ Cathode Materials Induced by the Initial Charge. *Chem. Mater.* **2014**, *26* (2), 1084−1092.

DOI: 10.1021/acsami.6b09585
ACS Appl. Mater. Interfaces 2016, 8, 27762−27771

(9) Abraham, D. P.; Twesten, R. D.; Balasubramanian, M.; Petrov, I.; McBreen, J.; Amine, K. Surface Changes on $LiNi_{0.8}Co_{0.2}O_2$ Particles during Testing of High-Power Lithium-Ion Cells. *Electrochem. Commun.* **2002**, *4* (8), 620−625.
(10) Robert, R.; Bünzli, C.; Berg, E. J.; Novák, P. Activation Mechanism of $LiNi_{0.80}Co_{0.15}Al_{0.05}O_2$: Surface and Bulk Operando Electrochemical, Differential Electrochemical Mass Spectrometry, and X-ray Diffraction Analyses. *Chem. Mater.* **2015**, *27* (2), 526−536.
(11) Zhang, S. S. Insight into the Gassing Problem of Li-Ion Battery. *Front. Energy Res.* **2014**, *2*, 59.
(12) Matsumoto, K.; Kuzuo, R.; Takeya, K.; Yamanaka, A. Effects of CO_2 in Air on Li Deintercalation from $LiNi_{1-x-y}Co_xAl_yO_2$. *J. Power Sources* **1999**, *81*−*82*, 558−561.
(13) Liu, H. S.; Zhang, Z. R.; Gong, Z. L.; Yang, Y. Origin of Deterioration for $LiNiO_2$ Cathode Material during Storage in Air. *Electrochem. Solid-State Lett.* **2004**, *7* (7), A190−A193.
(14) Nam, K.-W.; Bak, S.-M.; Hu, E.; Yu, X.; Zhou, Y.; Wang, X.; Wu, L.; Zhu, Y.; Chung, K.-Y.; Yang, X.-Q. Combining In Situ Synchrotron X-Ray Diffraction and Absorption Techniques with Transmission Electron Microscopy to Study the Origin of Thermal Instability in Overcharged Cathode Materials for Lithium-Ion Batteries. *Adv. Funct. Mater.* **2013**, *23* (8), 1047−1063.
(15) Hwang, S.; Kim, S. M.; Bak, S.-M.; Cho, B.-W.; Chung, K. Y.; Lee, J. Y.; Chang, W.; Stach, E. A. Investigating Local Degradation and Thermal Stability of Charged Nickel-Based Cathode Materials through Real-Time Electron Microscopy. *ACS Appl. Mater. Interfaces* **2014**, *6* (17), 15140−15147.
(16) Wang, L.; Maxisch, T.; Ceder, G. A First-Principles Approach to Studying the Thermal Stability of Oxide Cathode Materials. *Chem. Mater.* **2007**, *19* (3), 543−552.
(17) Park, M.; Zhang, X.; Chung, M.; Less, G. B.; Sastry, A. M. A Review of Conduction Phenomena in Li-Ion Batteries. *J. Power Sources* **2010**, *195* (24), 7904−7929.
(18) Jinschek, J. R. Advances in the Environmental Transmission Electron Microscope (ETEM) for Nanoscale in Situ Studies of Gas-Solid Interactions. *Chem. Commun.* **2014**, *50* (21), 2696−2706.
(19) DENSsolutions. *DENS EMheaterchips*, http://www.denssolutions.com/ (accessed Jan. 1, 2016).
(20) Zheng, S.; Huang, R.; Makimura, Y.; Ukyo, Y.; Fisher, C. A. J.; Hirayama, T.; Ikuhara, Y. Microstructural Changes in $LiNi_{0.8}Co_{0.15}Al_{0.05}O_2$ Positive Electrode Material during the First Cycle. *J. Electrochem. Soc.* **2011**, *158* (4), A357−A362.
(21) Reed, J.; Ceder, G.; Van Der Ven, A. Layered-to-Spinel Phase Transition in Li_XMnO_2. *Electrochem. Solid-State Lett.* **2001**, *4* (6), A78−A81.
(22) de Groot, F. M. F.; Grioni, M.; Fuggle, J. C.; Ghijsen, J.; Sawatzky, G. A.; Petersen, H. Oxygen 1s X-Ray-Absorption Edges of Transition-Metal Oxides. *Phys. Rev. B: Condens. Matter Mater. Phys.* **1989**, *40* (8), 5715−5723.
(23) Yoon, W.-S.; Chung, K. Y.; McBreen, J.; Fischer, D. A.; Yang, X.-Q. Electronic Structural Changes of the Electrochemically Li-Ion Deintercalated $LiNi_{0.8}Co_{0.15}Al_{0.05}O_2$ Cathode Material Investigated by X-Ray Absorption Spectroscopy. *J. Power Sources* **2007**, *174* (2), 1015−1020.
(24) Wang, F.; Malac, M.; Egerton, R. F. Alternative Methods of Identifying the Oxidation of Metallic Nanoparticles Embedded in a Matrix. *Micron* **2007**, *38* (4), 371−376.
(25) Leapman, R. D.; Grunes, L. A.; Fejes, P. L. Study of the L 23 Edges in the 3 D Transition Metals and Their Oxides by Electron-Energy-Loss Spectroscopy with Comparisons to Theory. *Phys. Rev. B: Condens. Matter Mater. Phys.* **1982**, *26* (2), 614.
(26) Graetz, J.; Ahn, C. C.; Ouyang, H.; Rez, P.; Fultz, B. White Lines and d-Band Occupancy for the 3d Transition-Metal Oxides and Lithium Transition-Metal Oxides. *Phys. Rev. B: Condens. Matter Mater. Phys.* **2004**, *69* (23), 235103.
(27) Riedl, T.; Gemming, T.; Wetzig, K. Extraction of EELS White-Line Intensities of Manganese Compounds: Methods, Accuracy, and Valence Sensitivity. *Ultramicroscopy* **2006**, *106* (4−5), 284−291.
(28) Sigle, W. ANALYTICAL TRANSMISSION ELECTRON MICROSCOPY. *Annu. Rev. Mater. Res.* **2005**, *35* (1), 239−314.
(29) Conry, T. E.; Mehta, A.; Cabana, J.; Doeff, M. M. XAFS Investigations of $LiNi_{0.45}Mn_{0.45}Co_{0.1-y}Al_yO_2$ Positive Electrode Materials. *J. Electrochem. Soc.* **2012**, *159* (9), A1562−A1571.
(30) Qian, D.; Xu, B.; Chi, M.; Meng, Y. S. Uncovering the Roles of Oxygen Vacancies in Cation Migration in Lithium Excess Layered Oxides. *Phys. Chem. Chem. Phys.* **2014**, *16* (28), 14665−14668.
(31) Rask, J. H.; Miner, B. A.; Buseck, P. R. Determination of Manganese Oxidation States in Solids by Electron Energy-Loss Spectroscopy. *Ultramicroscopy* **1987**, *21* (4), 321−326.
(32) Jeangros, Q.; Hansen, T. W.; Wagner, J. B.; Damsgaard, C. D.; Dunin-Borkowski, R. E.; Hébert, C.; Van herle, J.; Hessler-Wyser, A. Reduction of Nickel Oxide Particles by Hydrogen Studied in an Environmental TEM. *J. Mater. Sci.* **2013**, *48* (7), 2893−2907.
(33) De Jonghe, L. C.; Chang, M. Surface Oxygen Chemical Potential in a Gas-Solid Reaction. *J. Electrochem. Soc.* **1983**, *130* (11), 2263−2266.
(34) Reuter, K.; Scheffler, M. Composition, Structure, and Stability of RuO_2(110) as a Function of Oxygen Pressure. *Phys. Rev. B: Condens. Matter Mater. Phys.* **2001**, *65* (3), 035406.
(35) Akiba, K.; Ueda, M.; Kawamura, K.; Maruyama, T. Continuous Monitoring of Oxygen Chemical Potential at the Surface of Growing Oxide Scales during High Temperature Oxidation of Metals. *Mater. Trans.* **2008**, *49* (3), 629−636.
(36) Parravano, G. The Reduction of Nickel Oxide by Hydrogen. *J. Am. Chem. Soc.* **1952**, *74* (5), 1194−1198.
(37) Basu, J.; Divakar, R. In-Situ Electron Microscopy Investigation of Reduction-Induced Microstructural Changes in NiO. *Ceram. Int.* **2015**, *41* (10A), 12658−12667.
(38) Ostyn, K. M.; Carter, C. B. On the Reduction of Nickel Oxide. *Surf. Sci.* **1982**, *121* (3), 360−374.
(39) Madec, L.; Xia, J.; Petibon, R.; Nelson, K. J.; Sun, J.-P.; Hill, I. G.; Dahn, J. R. Effect of Sulfate Electrolyte Additives on $LiNi_{1/3}Mn_{1/3}Co_{1/3}O_2$/Graphite Pouch Cell Lifetime: Correlation between XPS Surface Studies and Electrochemical Test Results. *J. Phys. Chem. C* **2014**, *118* (51), 29608−29622.
(40) Kim, Y. J.; Cho, J.; Kim, T.-J.; Park, B. Suppression of Cobalt Dissolution from the $LiCoO_2$ Cathodes with Various Metal-Oxide Coatings. *J. Electrochem. Soc.* **2003**, *150* (12), A1723−A1725.
(41) Qiu, B.; Zhang, M.; Wu, L.; Wang, J.; Xia, Y.; Qian, D.; Liu, H.; Hy, S.; Chen, Y.; An, K.; Zhu, Y.; Liu, Z.; Meng, Y. S. Gas−solid Interfacial Modification of Oxygen Activity in Layered Oxide Cathodes for Lithium-Ion Batteries. *Nat. Commun.* **2016**, *7*, 12108.
(42) Hwang, S.; Kim, S. Y. M.; Bak, S.-M.; Kim, S. Y. M.; Cho, B.-W.; Chung, K. Y.; Lee, J. Y.; Stach, E. A.; Chang, W. Using Real-Time Electron Microscopy To Explore the Effects of Transition-Metal Composition on the Local Thermal Stability in Charged $Li_xNi_yMn_zCo_{1-y-z}O_2$ Cathode Materials. *Chem. Mater.* **2015**, *27* (11), 3927−3935.
(43) Gu, M.; Belharouak, I.; Genc, A.; Wang, Z.; Wang, D.; Amine, K.; Gao, F.; Zhou, G.; Thevuthasan, S.; Baer, D. R.; Zhang, J.-G.; Browning, N. D.; Liu, J.; Wang, C. Conflicting Roles of Nickel in Controlling Cathode Performance in Lithium Ion Batteries. *Nano Lett.* **2012**, *12* (10), 5186−5191.

DOI: 10.1021/acsami.6b09585
ACS Appl. Mater. Interfaces 2016, 8, 27762−27771